Circadian lipid synthesis in brown fat maintains murine body temperature during chronic cold

Marine Adlanmerini[a,b], Bryce J. Carpenter[a,b], Jarrett R. Remsberg[a,b], Yann Aubert[a,b], Lindsey C. Peed[a,b], Hannah J. Richter[a,b,c], and Mitchell A. Lazar[a,b,1]

[a]Institute for Diabetes, Obesity, and Metabolism, University of Pennsylvania Perelman School of Medicine, Philadelphia, PA 19104; [b]Division of Endocrinology, Diabetes, and Metabolism, Department of Medicine, University of Pennsylvania Perelman School of Medicine, Philadelphia, PA 19104; and [c]Biochemistry and Molecular Biophysics Graduate Group, University of Pennsylvania, Philadelphia, PA 19104

Ambient temperature influences the molecular clock and lipid metabolism, but the impact of chronic cold exposure on circadian lipid metabolism in thermogenic brown adipose tissue (BAT) has not been studied. Here we show that during chronic cold exposure (1 wk at 4 °C), genes controlling de novo lipogenesis (DNL) including *Srebp1*, the master transcriptional regulator of DNL, acquired high-amplitude circadian rhythms in thermogenic BAT. These conditions activated mechanistic target of rapamycin 1 (mTORC1), an inducer of *Srebp1* expression, and engaged circadian transcriptional repressors REV-ERBα and β as rhythmic regulators of *Srebp1* in BAT. SREBP was required in BAT for the thermogenic response to norepinephrine, and depletion of SREBP prevented maintenance of body temperature both during circadian cycles as well as during fasting of chronically cold mice. By contrast, deletion of REV-ERBα and β in BAT allowed mice to maintain their body temperature in chronic cold. Thus, the environmental challenge of prolonged noncircadian exposure to cold temperature induces circadian induction of SREBP1 that drives fuel synthesis in BAT and is necessary to maintain circadian body temperature during chronic cold exposure. The requirement for BAT fatty acid synthesis has broad implications for adaptation to cold.

circadian | thermogenesis | body temperature | brown adipose tissue

Circadian rhythms orchestrate numerous physiological processes and behaviors, allowing coordinated anticipation and adaptation to environmental challenges. Several external environmental cues entrain the central and peripheral clocks including food availability, light, and temperature (1). The perturbation of these zeitgebers can induce pathologic misalignments that predispose both humans and mice to metabolic disorders including obesity and type 2 diabetes, hypertension, and cancer (2–4).

Homeostatic regulation of body temperature in response to cold environments is controlled by thermogenic brown adipose tissue (BAT), particularly in rodents, although it is increasingly clear that humans have functional brown adipocytes (5, 6). Circadian rhythm of BAT activity regulates circadian body temperature and circadian cold sensitivity (7–11), allowing mammals to live in near-freezing temperature by a profound remodeling of lipid metabolism and an impressive increase in metabolic rate and heat production (12–14). Time-of-day modulation of substrate mobilization and oxidation during acute cold exposure has been reported (8), but the impact of chronic cold exposure on circadian regulation of lipid metabolism in BAT has not been explored to date.

We recently noted that long-term exposure to an obesogenic diet amplified and synchronized circadian rhythms of genes controlling fat synthesis and oxidation in liver, without a similar effect in adipose tissue (15), indicating that chronic noncircadian environmental challenges can alter circadian metabolism in a tissue-specific manner. Here we have investigated the effect of constant, chronic cold temperature on circadian rhythms of gene expression. Remarkably, expression of genes critical for fatty acid oxidation (FAO) and de novo lipogenesis (DNL) gene expression,

as well as the master transcriptional regulator of DNL, *Srebp1*, acquired high-amplitude circadian rhythms in BAT, but not in liver upon chronic cold exposure. These conditions activated mechanistic target of rapamycin 1 (mTORC1), an inducer of *Srebp1* expression, and engaged circadian transcriptional repressors REV-ERBα and β as rhythmic regulators of *Srebp1*. Moreover, we show that BAT SREBP activity was necessary for maximal thermogenic capacity and maintenance of body temperature during the light phase and fasting.

Results

Chronic Cold Exposure Induces Synchronous High-Amplitude Circadian Rhythms of Lipolytic, Fatty Acid Oxidation, and De Novo Lipogenic Genes in BAT.

To determine how chronic environmental stress affects circadian rhythmicity of lipid metabolism in thermogenic BAT, C57BL/6J mice were housed for 1 wk at 4 °C in regular 12:12-h light–dark conditions. In this setting, mice maintained their body weight (*SI Appendix*, Fig. S1A), with increased BAT mass (*SI Appendix*, Fig. S1B). As expected (13, 16, 17), genes

Significance

Circadian coordination of food availability, energy expenditure, and lipid metabolism is crucial for metabolic adaptation to environmental challenges. Here, we demonstrate that chronic cold temperature causes new circadian rhythms of de novo lipogenesis in brown adipose tissue (BAT). These cyclic changes are caused by a cold-induced rhythm of transcription factor SREBP1c, which is required for maximal thermogenesis and maintenance of body temperature both at the time of the physiological circadian trough as well as when food is unavailable during chronic cold exposure. Our findings demonstrate the circadian plasticity of lipid metabolism in BAT during chronic cold and the unexpected requirement of fatty acid synthesis for chronic maintenance of thermogenesis, suggesting strategies for increasing energy expenditure to combat metabolic diseases.

PHYSIOLOGY

involved in intracellular lipolysis and FAO were induced by prolonged exposure at 4 °C (Fig. 1*A*). Compared with mice housed at thermoneutrality, both lipolytic and FAO gene expression acquired a high-amplitude circadian rhythm in BAT of mice subject to chronic cold, with peak expression at ZT16 (Fig. 1*A*). Unexpectedly, however, genes controlling de novo lipogenesis (DNL) were massively induced by chronic cold exposure, with a circadian rhythm that also peaked at ZT16 in-phase with FAO genes (Fig. 1*B*). The increased rhythmic expression of key DNL enzymes ACC (*SI Appendix*, Fig. S1*C*) and FASN (*SI Appendix*, Fig. S1*D*) were also reflected at the protein level. The massive induction of both FAO and DNL genes programmed by chronic cold exposure resulted in an overall decrease in BAT triglyceride content after chronic cold exposure as observed by Hematoxylin and Eosin (H&E) staining (*SI Appendix*, Fig. S1*E*). The accumulation of triglycerides (TG) observed at 29 °C during the light phase is no longer observed during chronic cold housing (*SI Appendix*, Fig. S1*F*), suggesting a complete esterification and oxidation of newly synthesized fatty acid rather than a storage in lipid droplets. In contrast to the BAT, the expression and circadian amplitude of DNL genes were markedly reduced in livers of the same mice exposed to chronic cold (*SI Appendix*, Fig. S2*A*).

In response to cold, s.c. inguinal white adipose tissue (iWAT) undergoes a process termed "browning," during which adipocytes develop multilocular lipid droplets and thermogenic capacity (18, 19). Indeed, similar to BAT, DNL gene expression also acquired a high-amplitude circadian rhythm in iWAT of WT mice housed 1 wk at 4 °C compared to WT mice housed 1 wk at 29 °C (*SI Appendix*, Fig. S2*B*). Thus, BAT and iWAT, the tissues critical for maintaining body temperature homeostasis during environmental perturbation, shared the chronic cold-induced high-amplitude circadian rhythms of genes controlling DNL. FAO gene expression was also induced in iWAT but did not acquire a statistically significant circadian rhythm (*SI Appendix*, Fig. S2*C*).

Master Transcriptional Regulator of DNL, *Srebp1c*, Acquires a High-Amplitude Rhythm in BAT of Chronic Cold-Exposed Mice. We next evaluated the expression of *Srebp1*, a master regulator of DNL gene expression (20, 21). Both *Srebp1a* and *Sprebp1c* were markedly induced with a high-amplitude circadian rhythm (Fig. 2*A*). SREBP1 protein expression also acquired a new circadian rhythm after chronic cold exposure, with a peak at ZT10 for the full-length form and at ZT16 for the active nuclear-cleaved form of SREBP1 (Fig. 2*B*). Nuclear SREBP1 activates *Srebp1* gene expression (22), likely magnifying the circadian rhythm of *Srebp1* mRNA and potentially accounting for the finding that peak SREBP protein levels precede the peak of *Srebp* and DNL gene expression. Carbohydrate response element binding protein (*Chrebp*) *β*, a SREBP1-gene target that is also a transcriptional activator of DNL genes also acquired a marked circadian rhythm in chronic cold (*SI Appendix*, Fig. S2*D*).
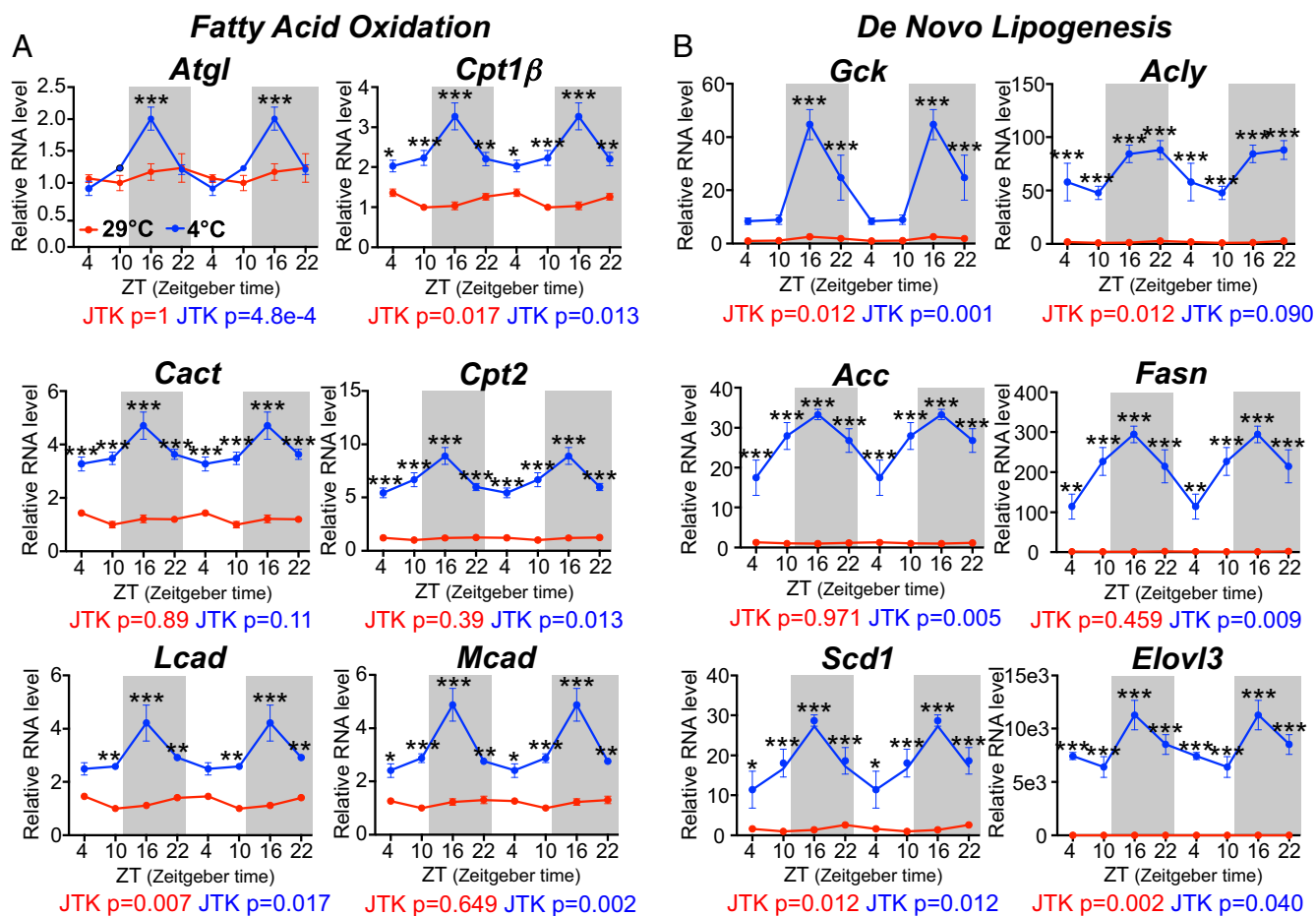
Fig. 1. Lipolytic, fatty acid oxidation (FAO), and de novo lipogenesis (DNL) genes acquire high-amplitude circadian rhythms in BAT of mice exposed to 4 °C for 1 wk. (*A*) Lipolytic and FAO circadian gene expression in BAT from WT mice housed 1 wk at 29 °C or 4 °C. (*B*) DNL circadian gene expression in BAT from WT mice housed 1 wk at 29 °C or 4 °C. Results were compared by 2-way ANOVA (n = 5 to 6 per group). Statistical significance of rhythmicity was determined using JTK_CYCLE (56). *P < 0.5, **P < 0.1, ***P < 0.001.

Fig. 2. *Srebp1* acquires high-amplitude circadian rhythms in thermogenic BAT after chronic cold exposure. (*A*) *Srebp1a* and *Srebp1c* circadian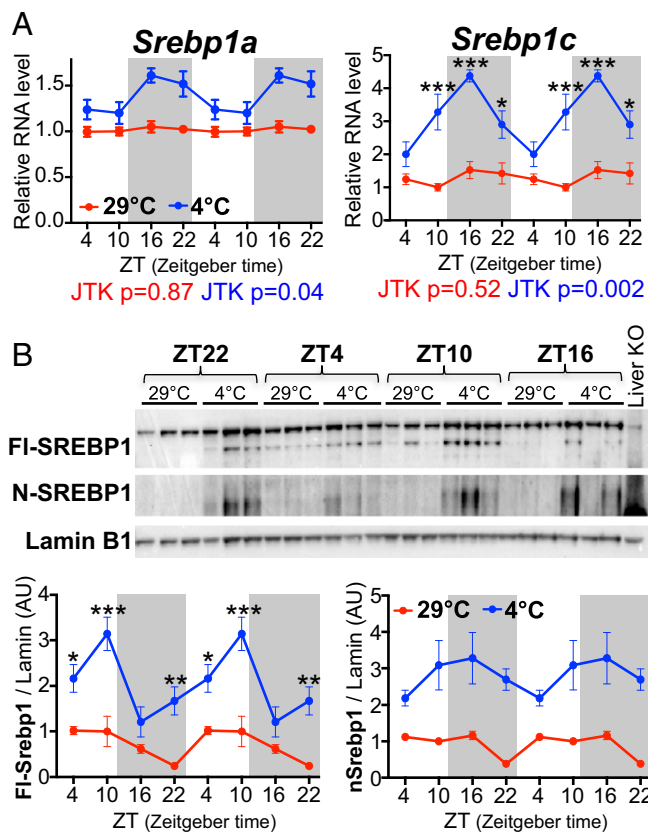 gene expression in BAT from WT mice housed 1 wk at 29 °C or 4 °C. (*B*) Circadian expression of full-length (Fl-SREBP1) and nuclear-cleaved SREBP1c (N-SREBP1) protein in BAT from WT mice housed 1 wk at 29 °C or 4 °C. Liver SCAP-KO sample is used as negative control. The results were compared by 2-way ANOVA (*n* = 3 to 6 per group). Statistical significance of rhythmicity was determined using JTK_CYCLE (56). *$P < 0.5$, **$P < 0.1$, ***$P < 0.001$.

Since SREBP1c cleavage is regulated by insulin (23–25), we considered whether insulin contributes to the high rhythm acquired by *Srebp1* during chronic cold exposure. However, although mice exposed to chronic cold ate more (*SI Appendix*, Fig. S3A) and consumed a higher percentage of their total food intake during the light phase than mice housed at 29 °C (*SI Appendix*, Fig. S3B), serum insulin levels were similar at both 29 °C and 4 °C (*SI Appendix*, Fig. S3C).

Circadian Nuclear Receptors REV-ERBα and REV-ERBβ Regulate *Srebp1*/DNL Gene Expression in BAT. To delineate the mechanisms initiating the high-amplitude circadian rhythm of the SREBP1/DNL pathway in chronic cold, we turned our attention to the circadian nuclear receptor REV-ERBα, which controls circadian thermogenesis in response to acute cold (7). We noted that while REV-ERBα remained circadian in BAT during chronic cold exposure, its expression was phase-advanced from ZT10-ZT16 during housing at 29 °C to ZT4-ZT10 after housing at 4 °C (Fig. 3A and *SI Appendix*, Fig. S4A). The altered circadian phase of REV-ERBα expression was mirrored by *Bmal1*, the circadian clock gene that is canonically repressed by REV-ERBα, whose anti-phase expression was also phase-advanced by chronic cold exposure (Fig. 3B). Importantly, the phase-advanced REV-ERBα expression at 4 °C matched the trough of the high-amplitude circadian rhythm of *Srebp1* expression.

To better explore the role of REV-ERBα in BAT, we used CRISPR/Cas9 to generate a C57BL/6 mouse model in which a

3xHA epitope tag was knocked into the germline in frame with the REV-ERBα N terminus (herein referred to as HA-REV-ERBα mice) (Fig. 3C). This model allows immunodetection and immunoprecipitation of endogenous REV-ERBα protein using a highly specific HA antibody with less background than can be achieved with currently available antibodies to REV-ERBα. Expression of HA-REV-ERBα recapitulated that of wild type, as it was circadian in BAT from HA-epitope–tagged mice housed at room temperature with maximal expression observed at ZT10 (*SI Appendix*, Fig. S4B). HA-ChIP-seq was performed on BAT harvested at ZT10 (26), when HA-REV-ERBα levels were comparable after 1 wk at 4 °C versus 29 °C (*SI Appendix*, Fig. S4C). The majority of REV-ERBα peaks were observed under both conditions, but 3,059 peaks were specific to the BAT from mice exposed to chronic cold (Fig. 3D), and the genes nearest these REV-ERBα binding sites were enriched for function in fatty acid and triacylglycerol metabolism (Fig. 3E). Notably, 4 °C-specific REV-ERBα binding sites were observed near *Srebf1* (*Srebp1c*) as well as at DNL genes including *Acly*, *Acaca* (ACC), *Fasn*, and *Scd1* (Fig. 3F), suggesting that REV-ERBα might directly control the expression of *Srebp1* and DNL genes.

To determine if these REV-ERBα binding sites were functional, we studied BAT from mice in which both REV-ERBα and its redundant isoform REV-ERBβ were deleted by crossing C57BL/6 mice expressing Cre recombinase in BAT (Ucp1-Cre) with C57/Bl6 mice whose REV-ERBα (*Nr1d1*) and β (*Nr1d2*) loci were floxed to enable conditional deletion (27). BAT from these REV-ERBα/β BAT double-knockout (DKO) mice was depleted of both *Rev-erbα* and *Rev-erbβ* (Fig. 3G and *SI Appendix*, Fig. S4D), and this had functional consequences including marked de-repression of REV-ERB target genes *Ucp1*, *Bmal1*, and *Npas2* (Fig. 4H). Moreover, consistent with the HA-REV-ERBα BAT cistrome and circadian expression, deletion of REV-ERBs increased the expression of *Srebp1c* and DNL genes expression in BAT of mice exposed to chronic cold temperatures at ZT10 (Fig. 3I). Together these data suggest that circadian repression by REV-ERBs triggers rhythmicity of *Srebp1*/DNL gene expression.

In addition to its acquired rhythmicity, the basal level of *Srepb1*/DNL gene expression was also increased in chronic cold. This was likely explained by the increased activity of the Srebp1 activator mTORC1 (28–30), as reflected by robust phosphorylation of mTORC1 target S6 in BAT from WT mice housed at 4 °C compared to BAT from WT mice housed at 29 °C (*SI Appendix*, Fig. S5A). Both acute and chronic cold exposures have previously been shown to activate mTORC1 (31–33); however, while β-adrenergic receptors *AdrB1* and *AdrB3* were circadian in chronic cold, the increased phosphorylation of S6 was not rhythmic. Together, these results suggest that chronic cold-induced mTORC1 activation set a high tone of *Srebp1*/DNL gene expression, which was repressed in a circadian manner by REV-ERBs.

SREBP Is Necessary for Chronic Cold-Induced DNL Gene Expression in BAT. We next assessed the importance of SREBP1 for the chronic cold-induced high-amplitude circadian rhythms of DNL genes in BAT by deleting SCAP, an adaptor protein that is required for the stability of ER-bound SREBP1 as well as for its insulin-stimulated proteolytic cleavage that regulates its translocation to the nucleus as a lipogenic transcription factor (25, 34). *Scap*^Flox/Flox^ mice were bred with Ucp1-CreER mice, and moxifen was given at 6 wk of age to induce BAT-specific deletion of *Srebp* in Cre-positive mice (SCAP BAT KO mice) (Fig. 4A). This resulted in markedly reduced gene expression of *Srebp1c* (Fig. 4B) and its active nuclear-cleaved SREBP1 protein product (Fig. 4C) compared to control mice subjected to 7 d of cold exposure at 12 wk of age.
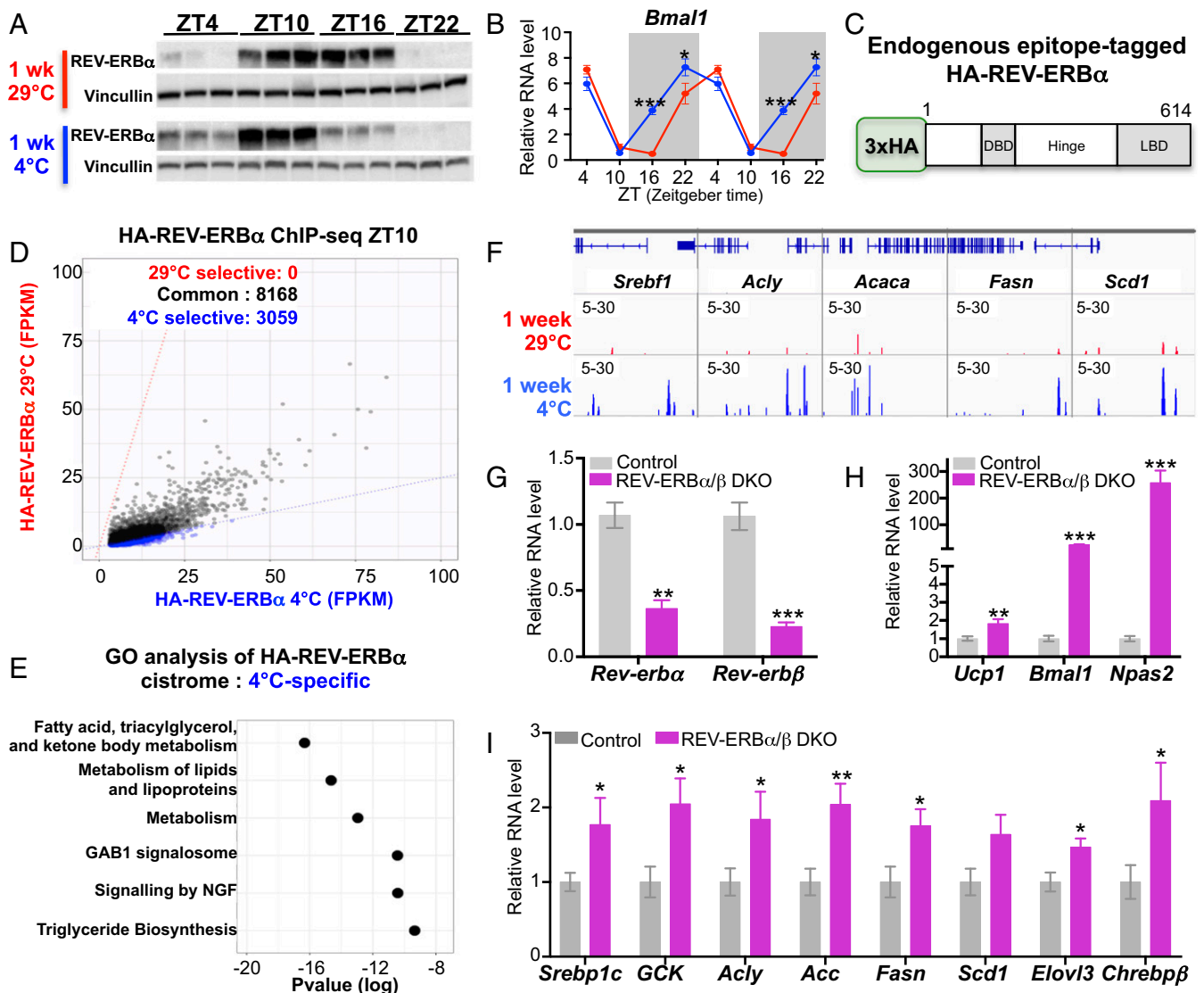
Fig. 3. The circadian nuclear receptor REV-ERB regulates SREBP/DNL gene expression in BAT. (*A*) Circadian expression of REV-ERBα after 1 wk at 29 °C or 1 wk at 4 °C (*n* = 3 per condition). (*B*) Circadian expression of *Bmal1* in BAT from WT mice housed 1 wk at 29 °C or 4 °C. The results were compared by 2-way ANOVA (*n* = 5 to 6 per group). (*C*) Endogenous HA-epitope–tagged REV-ERBα protein model. (*D*) ChIP-seq of BAT from HA-REV-ERBα mice, using HA antibody, comparing mice housed at thermoneutrality or 1 wk at 4 °C. Scatterplots of the HA-REV-ERBα cistrome in BAT at 29 °C (*y* axis) and 4 °C (*x* axis). The sites selective at 4 °C are plotted in blue, and the sites common at 29 °C and 4 °C are plotted in black. The cutoff for differentially regulated sites was a fold-change of >4 (*n* = 4 per group). (*E*) Gene ontology analysis of HA-REV-ERBα ChIP-seq peaks selective to BAT after 1 wk at 4 °C. (*F*) Genome browser view of HA-REV-ERBα ChIP-seq peaks in mice housed at 29 °C (red) and 4 °C (blue) near DNL genes. (*G*) *Rev-erbα* and *Rev-erbβ* gene expression in BAT from control (Cre-) and Rev-erbα/β DKO mice housed 1 wk at 4 °C (*n* = 3). (*H*) Canonical REV-ERB target genes expression in BAT from control (Cre-) and REV-ERB/β DKO mice housed 1 wk at 4 °C (*n* = 3). (*I*) DNL gene expression in BAT from control (Cre-) and REV-ERBα/β DKO mice housed 1 wk at 4 °C at ZT10 (*n* = 7 to 9 per group). In *G*–*I*, the results were compared by unpaired *t* test. *$P < 0.5$, **$P < 0.1$, ***$P < 0.001$.

Importantly, loss of SREBP1 activity markedly reduced DNL gene expression in BAT of chronically cold mice at ZT16 but not at ZT4 (Fig. 4*D*), and not in mice housed at thermoneutrality (*SI Appendix*, Fig. S6). BAT expression *of Chrebpβ* was also SCAP-dependent (*SI Appendix*, Fig. S7A), consistent with the conclusion that SREBP regulated *Chrebpβ* expression as previously described (35). In absence of SREBP, BAT mass was decreased (Fig. 4*E*), and BAT triglyceride levels were reduced (Fig. 4*F*), even below the already reduced level caused by chronic cold exposure of control mice. On the other hand, loss of SREBP activity in BAT during chronic cold exposure did not reduce the expression of *Ucp1* (*SI Appendix*, Fig. S7B) nor genes involved in oxidative phosphorylation (*SI Appendix*, Fig. S7C), FAO (*SI Appendix*, Fig. S7D), or fatty acid uptake (*SI Appendix*, Fig. S7E).

We also considered whether iWAT, which becomes brown-like during cold exposure, was contributing to the phenotype of the SCAP BAT KO mice. Consistent with previous observations (36), Ucp1-CreER was expressed at very low levels in iWAT relative to intrascapular BAT, even following cold exposure (*SI Appendix*, Fig. S8A). iWAT expression of *Scap* mRNA (*SI Appendix*, Fig. S8B) as well as DNL genes (*SI Appendix*, Fig. S8C) were barely affected in these SCAP BAT KO mice which had received tamoxifen 6 wk prior to cold exposure. Moreover, iWAT weight (*SI Appendix*, Fig. S8D) and expression of brown-like genes including *Ucp1* (*SI Appendix*, Fig. S8E) were similar in control and SCAP BAT KO mice after chronic cold exposure. These results strongly suggest that intrascapular BAT, rather than brown-like adipocytes in iWAT, was responsible for the
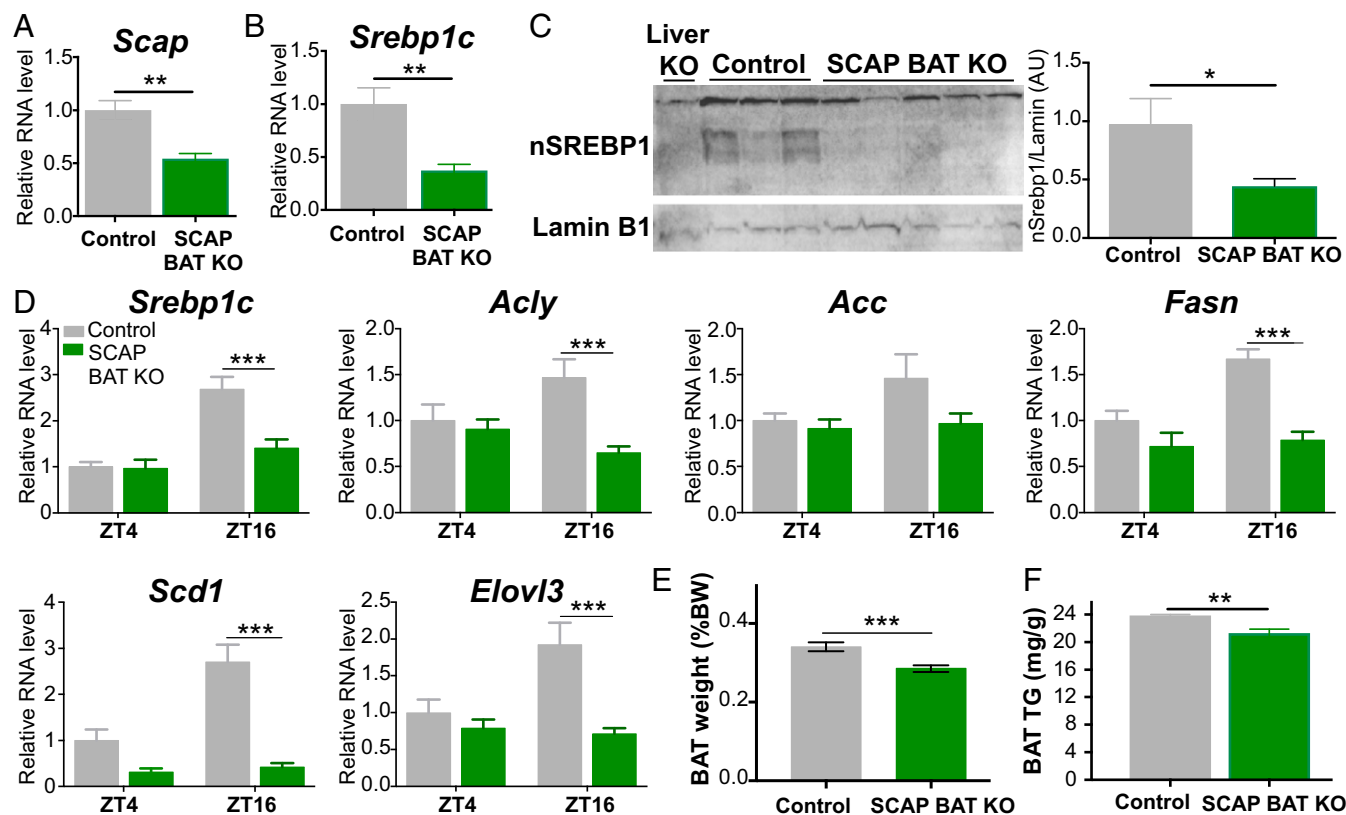
Fig. 4. SREBP function in BAT is necessary to induce DNL during chronic cold exposure. (*A*) *Scap*, (*B*) *Srebp1c* gene expression, and (*C*) detection of nuclear-cleaved nSREBP1 protein at ZT16 in BAT from control (ScapFlox/Flox) or SCAP BAT KO (ScapFlox/Flox-Ucp1CreER+) treated with tamoxifen at 6 wk of age and housed for 1 wk at 4 °C beginning at 12 wk of age. Liver SCAP-KO sample was used as negative control in *C*. The results were compared by unpaired *t* test (*n* = 3 to 5 per group). (*D*) DNL gene expression at ZT4 or ZT16 in BAT from control or SCAP BAT KO mice housed 1 wk at 4 °C. The results were compared by 2-way ANOVA (*n* = 7 to 12 per group). (*E*) BAT weight from control or SCAP BAT KO mice housed 1 wk at 4 °C. The results were compared by unpaired *t* test (*n* = 22 to 26 per group). (*F*) Triglycerides (TG) in BAT from control or SCAP BAT KO mice housed 1 wk at 4 °C. Measurements were performed at ZT4. The results were compared by unpaired *t* test (*n* = 4 per group). *$P < 0.5$, **$P < 0.1$, ***$P < 0.001$.

metabolic phenotype observed in the $Scap^{Flox/Flox}$-Ucp1-CreER mice.

SREBP Function in BAT Is Necessary for Maximal Thermogenic Capacity during Chronic Cold Exposure. We next tested whether SREBP activity in BAT was necessary for heat production and oxygen consumption (VO_2) during chronic cold exposure. Remarkably, BAT SCAP-deficient mice exhibited markedly lower basal and norepinephrine (NE)-stimulated VO_2 after 1 wk at 4 °C but not at thermoneutrality (29 °C) (Fig. 5 *A–C*). Similarly, basal and NE-stimulated heat production were impaired in BAT SCAP-deficient mice housed for 1 wk at 4 °C, but again, not at thermoneutrality (Fig. 5 *D–F*), consistent with a reliance on the DNL pathway in the adaptation to the chronic cold environment. Importantly, NE treatment induced *Ucp1* (*SI Appendix*, Fig. S7F) and OXPHOS gene expression (*SI Appendix*, Fig. S7G) in both control and SCAP-deficient mice. Thus, SREBP1 activity was required for maximal thermogenic capacity, although it was not necessary for *Ucp1* induction by cold.

BAT SREBP Is Necessary for Maintenance of Body Temperature during the Circadian Cycle and Fasting. Given the unexpected importance of BAT SREBP1 for heat production in the setting of chronic cold exposure, we next assessed the role of BAT SREBP in body temperature homeostasis in the setting of this environmental challenge. During chronic cold (day 5/6), the body temperature of WT mice was increased during the light phase compared to mice housed at thermoneutrality, with dampened circadian

variation (Fig. 6 *A* and *B*). A decrease in amplitude between the nocturnal and diurnal body temperature during cold exposure has also been observed in adult mouse lemurs exposed 10 d at 12 °C (37) and in rats after acclimation to cold and hypoxic environments (38).

Remarkably, mice lacking SREBP in BAT displayed a marked decrease in the physiological trough in body temperature during the light phase (Fig. 6C). A second cohort of mice depleted of BAT SREBP also demonstrated reduced body temperature trough at ZT4, but not at ZT16 (Fig. 6D). Body temperatures of BAT SCAP-depleted mice reached their minimum at ZT4 and gradually returned to normal at the end of the light phase (Fig. 6C). Interestingly, BAT SCAP-depleted mice ate more during the light phase (*SI Appendix*, Fig. S9A), starting around ZT5 (*SI Appendix*, Fig. S9B). Moreover, BAT SCAP-depleted mice presented a concomitant increase in RER (Respiratory Exchange Ratio) during the light phase, reflecting an increase in carbohydrate being used as the predominant fuel source over lipid (*SI Appendix*, Fig. S9 *C* and *D*). Although the increase in RER was relatively small (+0.04), this represents approximately half of the effect observed on RER by chronic high-fat diet (39).

Several studies demonstrate that food consumption could compensate for thermogenic fuel depletion during cold exposure (40, 41), especially during the light phase (11, 42). Thus, to avoid any confounding effect of feeding, mice were housed at 4 °C for 1 wk with ad libitum access to food, then maintained in the cold environment under fasting conditions for 6 h, beginning at ZT1. Remarkably, fasted SCAP-deficient mice were rapidly unable to
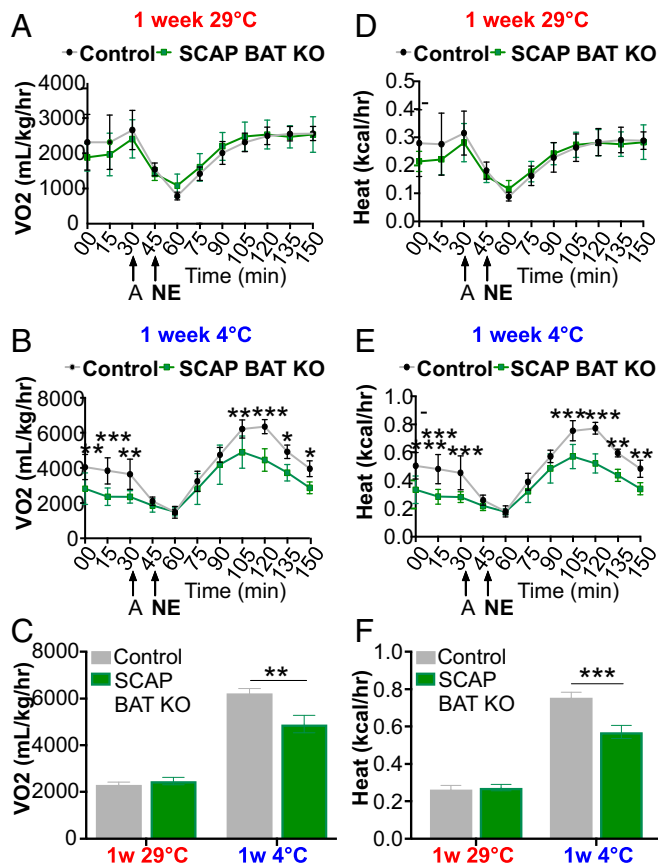
Fig. 5. Mice in chronic cold require SREBP function for maximal thermogenic capacity in response to norepinephrine. Thermogenic capacity of control or SCAP BAT KO mice in response to norepinephrine (NE) after 1 wk at 29 °C or 4 °C measured by oxygen consumption (*A–C*) and heat production (*D–F*). Time-course and direct comparison 1 h after NE injection. A, anesthesia. The results were compared by 2-way ANOVA (n = 5 to 7 per group). $*P < 0.5$, $**P < 0.1$, $***P < 0.001$.

maintain their body temperatures relative to control mice (Fig. 6*E*), suggesting that SCAP deficiency impaired thermogenesis by limiting energetic fuels rather than impairing thermogenic machinery. Thus, in chronic cold-exposed mice, the SREBP/DNL pathway in BAT was necessary to maintain body temperature during the circadian trough and upon fasting by providing fuel to sustain thermogenesis. However, opposite to the SCAP-deficient mice, REV-ERBα/β BAT DKO mice maintained their body temperatures longer than control mice during fasting in chronic cold (Fig. 6*F*), consistent with the absence of REV-ERBs activating the *SREBP*/DNL pathway as well as up-regulating uncoupling protein 1 (*Ucp1*).

Discussion

We have demonstrated that chronic cold exposure induces a profound remodeling of lipid metabolism in thermogenic BAT. Both DNL and FAO gene expression acquire high-amplitude circadian rhythms, as does the master lipogenic transcription factor SREBP1. During chronic cold housing, SREBP activity is necessary for DNL gene expression, maximal thermogenic capacity, and maintenance of body temperature during the light phase and fasting.

The high-amplitude circadian rhythms of DNL and FAO gene expression in BAT of mice exposed to chronic cold is reminiscent of the finding that chronic overnutrition induces in-phase circadian rhythms of DNL and FAO in liver (15) and suggests that

this adaptive mechanism may be a general feature of tissue-specific physiological responses to chronic metabolic challenges from the environment. In BAT, our results suggest that chronic cold exposure leads to a phase shift in expression and enhanced genomic binding of REV-ERBα that impose circadian rhythmicity on the expression of SREBP and its target genes that are simultaneously activated by the mTORC1 pathway (Fig. 7). We did not investigate the effect of rapamycin treatment on DNL during acute and chronic cold exposure because mTORC1 presents pleotropic effects, including mitochondrial biogenesis, oxidative metabolism, TCA, and nucleotide synthesis (33).

Our results demonstrate that BAT REV-ERBα and β regulated expression of SREBP1/DNL genes and allowed mice to maintain their body temperature during fasting in chronic cold exposure. The mechanisms underlying the changes in REV-ERB expression and genomic binding near metabolic circadian target genes during chronic cold exposure remain to be determined, but could indicate a role for cold-induced cooperating transcription or posttranslational modifications of REV-ERBα. Of note, the REV-ERBα/β deletion occurred during development (Ucp1-Cre), whereas SCAP deletion was induced in BAT by tamoxifen treatment prior to chronic cold exposure (Ucp1-CreER), such that Cre activity would not be increased in cold-induced BAT-like adipocytes in iWAT. Nevertheless, our findings demonstrate the circadian plasticity of lipid metabolism in BAT during chronic cold and, moreover, that DNL in BAT plays an important role in maintaining fuel sources under these conditions.

FAO is essential for BAT thermogenesis (13, 14, 43, 44), but the relative importance of circulating versus intracellular de novo synthesized lipids, as a fuel source, is not well understood. Previous studies have also demonstrated induction of DNL in thermogenic BAT (16, 17, 45–47). Here, we report that these changes in lipid metabolism are circadian. Moreover, our findings reveal a cold-induced circadian rhythm of SREBP1c by REV-ERBα that is required for the rhythmic increase in DNL genes, as well as Chrebpß, another powerful inducer of DNL (46).

Physiologically, SREBP was required for maintenance of body temperature during chronic cold exposure, both at the time of the physiological circadian trough as well as when food was unavailable. The reliance on increased DNL as a physiological adaptation to cold temperature reveals that two other well-known sources of fuel in BAT (i.e., fatty acids derived from lipolysis in WAT as well as glucose-generated electrons through glycolysis) are insufficient to maintain body temperature under these conditions. Of note, Guilherme et al. (48) recently demonstrated that DNL in BAT is not necessary to maintain euthermia during acute cold exposure. The present findings are consistent with these results, as the SCAP-deficient mice survived the acute phase of cold exposure in our studies. Interestingly, lipolytic regulators ATGL and CGI-58 have been found to be dispensable for BAT thermogenesis (41, 49), raising the possibility that newly synthesized SREBP/CHREBP-dependent fatty acids are directly oxidized.

Our findings of simultaneous induction of FAO and DNL are consistent with earlier studies showing that adrenergic stimulation induces both FAO and DNL (16, 17, 45–47). In their elegant studies, McGarry and Foster characterized simultaneous fatty acid synthesis and oxidation as a futile cycle that wastes energy and produces heat and suggested that this is prevented in liver by malonyl CoA inhibition of carnitine palmitoyltransferase 1 (50, 51). The mechanisms overriding malonyl CoA inhibition of CPT1 in BAT are not clear at this time. However, given the physiological role of BAT as a thermogenic organ, heat production by cycling of DNL and FAO could represent an adaptive response to chronic cold. Indeed, BAT lacking ANGPTL3/8 has recently been shown to exhibit simultaneous induction of DNL and FAO (52). Thus cold-induced synchronization of both DNL and FAO is likely an adaptive response to the high energy demand. The survival disadvantage of BAT-specific KO
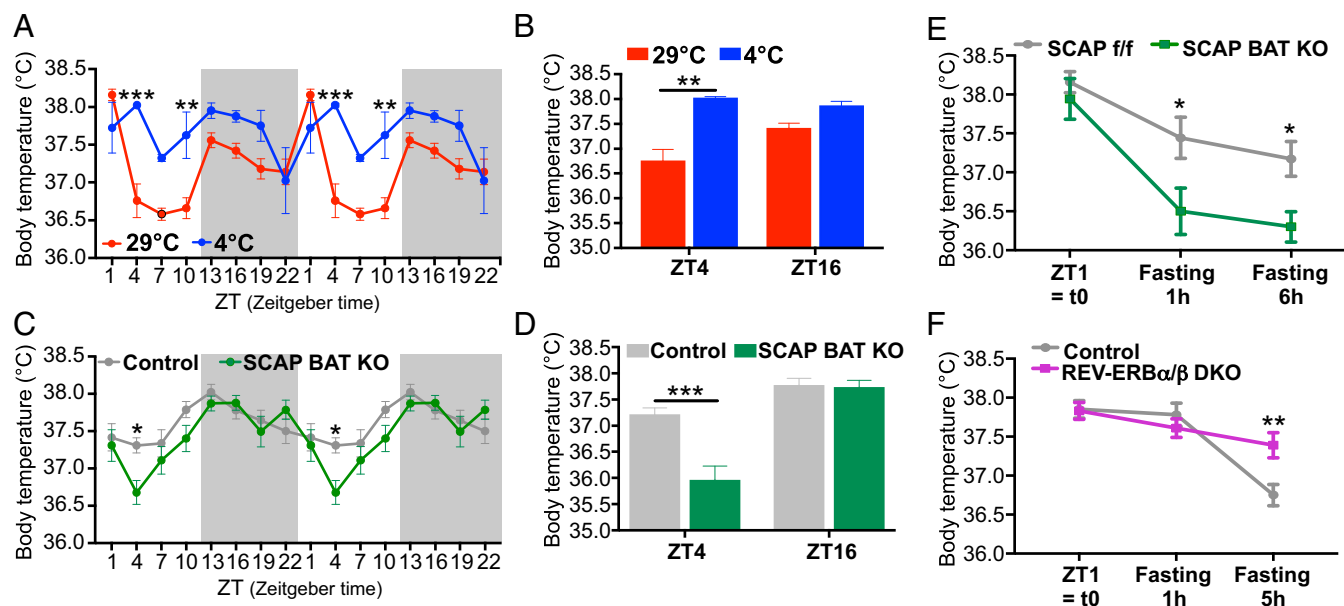
Fig. 6. Mice in chronic cold require SREBP function in BAT to maintain body temperature during circadian trough and fasting. (*A* and *B*) Body temperature of WT mice housed 1 wk at 29 °C or 4 °C. The results were compared by 2-way ANOVA (n = 4 to 5 per group). (*C* and *D*) Body temperature of control or SCAP BAT KO mice housed 1 wk at 4 °C. The results were compared by 2-way ANOVA (n = 12 to 14 per group, from 3 independent experiments). (*E*) Body temperature of control or SCAP BAT KO mice housed 1 wk at 4 °C and fasted from ZT1. The results were compared by 2-way ANOVA (n = 7 per group). (*F*) Body temperature of control and REV-ERBα/β DKO mice housed 1 wk at 4 °C and fasted from ZT1. The results were compared by 2-way ANOVA (n = 10 per group). *P < 0.5, **P < 0.1, ***P < 0.001.

of *Scap/Srebp* during fasting under chronic cold conditions strongly supports this hypothesis. The revelation that fatty acid synthesis in BAT is required for long-term adaptation to cold and could be a fuel source for BAT thermogenesis suggests strategies for increasing energy expenditure to combat metabolic diseases.

Methods

Mice. All animal studies were performed under protocols approved by the University of Pennsylvania Perelman School of Medicine Institutional Animal Care and Use Committee. Mice were group-housed in a temperature- and humidity-controlled, specific-pathogen–free animal facility at 22 °C under a 12:12-h light–dark cycle (lights on at 7 AM, lights off at 7 PM) with free access to standard chow (LabDiet, 5010) and water. All experiments were carried out on 11- to 14-wk-old male littermates.

Wild-type C57BL/6J male mice were obtained from Jackson Labs Technologies, Inc. *Scap*^Flox/Flox^ mice (25) were backcrossed to the C57BL/6J genetic background for at least 7 generations (kindly provided by Tim Osborne, Johns Hopkins All Children's Hospital, St. Petersburg, FL). *Scap*^Flox/Flox^ mice were bred to Ucp1-CreER mice on a C57BL/6J background [kindly provided by David Guertin, University of Massachusetts Medical School, Worcester, MA with generous permission from Christian Wolfrum, ETH Zürich, Zürich, Switzerland (35)]. To induce the expression of the Ucp1-CreER, 6-wk-old mice were injected i.p. for 5 d with 1.5 mg/mouse/day of tamoxifen dissolved in castor oil/ethanol (9:1 vol/vol). Both *Scap*^Flox/Flox^Ucp1-CreER+ and *Scap*^Flox/Flox^Ucp1-CreER- mice (control) were injected with tamoxifen. *Rev-erbα*^fl/fl^/*Rev-erbβ*^fl/fl^ mice (27) were bred to Ucp1-Cre mice maintained on a C57BL/6J background (Jackson Labs Technologies, Inc., B6.FVB-Tg[Ucp1-Cre]1Evdr/J, Stock 024670).

Generation of Epitope-Tagged REV-ERBα Mice by CRISPR. To generate Cas9 mRNA, a plasmid containing Cas9-HA-2NLS was linearized with XbaI (gift from Jorge Henao-Mejia, University of Pennsylvania Perelman School of Medicine, Philadelphia, PA). Approximately 1 μg of linearized plasmid was incubated with HiScribeTM T7 Quick High Yield RNA Synthesis kit (NEB #E2050S). RNA was purified using RNeasy mini columns (Qiagen #74106), and the capping reaction used Vaccinia Capping System (NEB #M2080S). RNA was purified using RNeasy Micro clean-up columns (Qiagen #74004). Capped Cas9 mRNA was then subject to polyadenylation (NEB #M0276S) and purified over a RNeasy Micro clean-up column and eluted in RNase-free water. Cas9 mRNA

integrity was validated using RNA BioAnalyzer. T7 promoter was added onto gRNA template targeting the ATG start site by PCR amplification using specific primers (targeting guide sequence: TGGTGAAGACATGACGACCC). The T7-sgRNA product was purified using a PCR purification kit (Qiagen) and used as the template for in vitro transcription using the MegaShortScript kit (Life Technologies) following the manufacturer's instructions. Subsequent sgRNA was purified using the MegaClear Kit (Life Technologies) and verified by RNA BioAnalyzer before dilution for microinjection. The ssDNA homology donor (IDT) containing the 3xHA tag was resuspended in water and prepared using DNA Clean and Concentrator (Zymo): A*G*T*TTGTGTCAAGGTC-CAGTTTGAATGACCGCTTTCAGCTGGTGAAGACATGTATCCATACGATGTTCCTG-ACTATGCGGGCTATCCCTATGACGTCCCGGACTATGCAGGATCGTATCCTTATGA-CGTTCCAGATTACGCTGGCACGACCCTCGACTCCAATAACAACACAGGTACTGA-GATTCTTATCTTTGCTC*T*G*T. Microinjection was performed by the Transgenic and Chimeric Mouse Facility at the University of Pennsylvania using C57BL/6J mice from JAX. Microinjection buffer consisted of 1 mM Tris pH 8.0, 0.1 mM EDTA, 100 ng/μL Cas9 mRNA, 50 ng/μL sgRNA, and 100 ng/μL of ssDNA homology donor. Insertion of epitope tag coding sequence was detected by PCR and confirmed by Sanger sequencing. HA-REV-ERBα mice were backcrossed to the C57BL/6J genetic background for at least 7 to 8 generations and genotyped using the PCR primers 5′-TAAGCCTTGGATGGAAATGG-3′ and 3′-AGCCACCCCAAGACCTTACT-5′.

Cold Exposure and Core Body Temperature Measurements. Mice acclimated at 22 °C were placed in single-housed cages at 4 to 5 °C or 29 °C for 1 wk. After 5 to 6 d in cold, rectal temperatures were recorded as previously described (53). For the fasting experiments in the cold, mice were housed for 6 d at 4 °C, and the food was removed for 5 to 6 h at ZT1 (8 AM) on day 7.

In Vivo Metabolic Phenotyping. Whole-body energy metabolism was evaluated using a Comprehensive Lab Animal Monitoring System (CLAMS, Columbia Instruments), as previously described (53). Mice maintained at 29 °C or 4 °C for 2 d were singly housed in metabolic chambers at 29 °C or 4 °C. Mice were acclimated for 48 h, and data were collected at days 5, 6, and 7 of thermoneutrality or cold housing.

Whole-Animal Energy Expenditure in Response to Norepinephrine. After housing at 29 °C or 4 °C during 1 wk of 12-wk-old male mice, oxygen-consumption rates and heat production were measured in response to
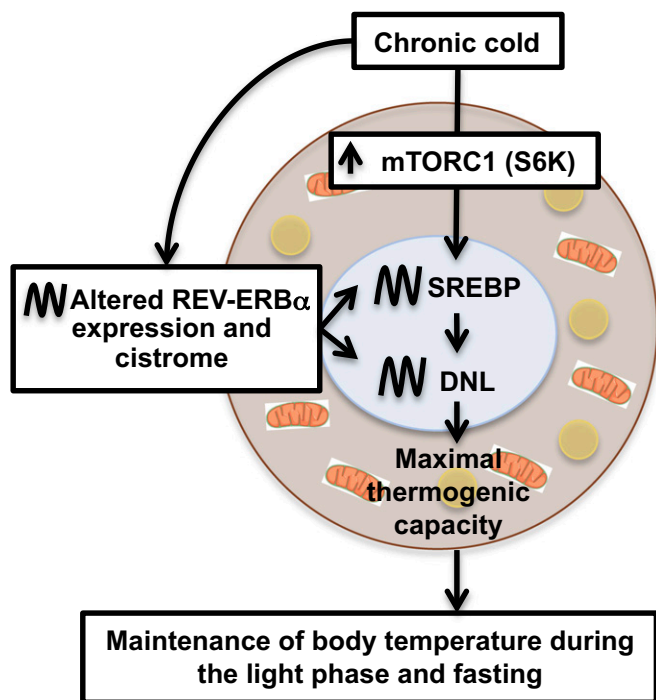
Fig. 7. Model depicting the circadian regulation of DNL by chronic cold exposure. In response to chronic cold stimulation, mTORC1 pathway is activated and triggers SREBP activity, as previously described (28–30). In parallel, chronic cold shift-advances REV-ERBα expression to the light phase and remodels its cistrome, targeting SREBP and DNL gene induction. Continuous activation of SREBP by mTORC1 combined with its circadian inhibition by REV-ERB results in the circadian expression of SREBP and DNL genes, which maximize thermogenic capacity and maintain body temperature during the light phase and fasting.

norepinephrine using Comprehensive Laboratory Animal Monitoring System (CLAMS, Columbus Instruments), as previously described (54).

RNA Isolation and Gene Expression Analysis (RT-qPCR). Total RNA was isolated from snap-frozen brown adipose tissue, white adipose tissue, and liver as previously described (53). All qPCR data were analyzed using a standard curve and normalized to 36B4 (Arbp) expression. Specific primer sequences are listed in *SI Appendix*, Table S1. For circadian gene expression, results are expressed relative to the mean of biological replicates at ZT10 29 °C, which was set to 1.

Western Blot. BAT samples were homogenized as previously described (53). For SREBP1, nuclear enrichment was performed in mouse BAT as previously described (55). Western blot images were images using Bio-Rad ChemiDoc Imaging Systems and analyzed by Image Lab software (v5.2). Antibodies used are listed in *SI Appendix*, Table S1.

Measurement of Triglycerides and Insulin. For TG measurement, brown adipose tissues were homogenized in lysis buffer (140 mM NaCl, 50 mM Tris pH 7.4, and 1% Triton X-100). TG concentration was then measured in both BAT and blood serum using the LiquiColor Triglyceride kit following the manufacturer's protocol (StanBio). Insulin was measured in blood serum using mouse ultrasensitive ELISA kit (Crystal Chem).

Histology. Histological procedures were performed as previously described (53) by the Penn Histology and Gene Expression Core.

Chromatin Immunoprecipitation. HA-REV-ERBα ChIP was performed as previously described (53). HA magnetic beads (Pierce, 88837) were used to perform the immunoprecipitation. For BAT ChIP-seq of HA-REV-ERBα, 4 biological replicates ChIPs were pooled for sequencing, and WT mice were used as negative control. The Chip-seq library has been performed as previously described (53).

ChIP-seq Data Analysis. Sequencing reads of individual biological replicates were aligned to the mouse mm9 genome build using bowtie2-2.1.0, allowing for one mismatch (-N1) and reporting the best alignment (-k1). Tag directories were generated from alignment files using homer-v4.10.1, with a fragment length of 150 base pairs, allowing a maximum of 1 tag per base pair to remove redundant reads. Tag directories from individual replicates were pooled together to generate pooled tag directories without the -tbp 1 option. Peaks were called with homer-v4.10.1 findPeaks with default parameters using the corresponding pooled WT samples as input. Visualization tracks were generated using homer-v4.10.1 with the following parameters (-fsize 5e7, -tbp 1, -res 1, -norm 3e7) and by subtracting the corresponding WT inputs. To retrieve the most significant peaks, peaks called on pooled tag directories were annotated using homer-v4.10.1 annotatePeaks, and tags were counted in pooled tag directories and reported as Fragments Per Kilobase per Million reads (FPKM). Annotated peak files were filtered using R and RStudio (R version 3.5.0 [2018-04-23], Platform: x86_64-apple-darwin15.6.0 [64-bit], Running under: macOS Sierra 10.12.6) to retrieve peaks with an FPKM value greater than 3. For the scatterplot analysis, annotated peaks were transposed to a bed format using homer-v4.10.1 pos2bed Perl script. The resulting files were concatenated, sorted, and merged using a custom script using bedTools v2.27.1, using a maximum merging distance of 100 base pairs. The resulting file was then annotated using homer-v4.10.1 annotatePeaks using the mouse mm9 genome build as a reference genome, and tags were counted in pooled tag directories and reported as FPKM. Peaks were deemed as shared or selective for one or the other condition based on an HA FPKM/WT FPKM ratio. Genome-browser tracks were generated with IGV 2.3.92. ChIP-seq data have been deposited to Gene Expression Omnibus under accession number GSE128960.

Quantification and Statistical Analysis. Data are presented as means ± SEM. To facilitate reading, circadian measurements (gene expression, protein quantification, TG, and insulin levels) were double-plotted. To characterize circadian rhythm in gene expression data, 4-time point datasets were analyzed using JTK_CYCLE (56). As indicated in the respective figure legends, statistical analyses were performed using unpaired 2-tailed t test for comparisons between 2 groups or 2-way analysis of variance (ANOVA) for assessment of variables effects (time, temperature, genotype), with multiple comparisons (Sidak's multiple comparisons test). All of the statistical analyses were performed with GraphPad Prism software (*$P < 0.5$, **$P < 0.1$, ***$P < 0.001$). RStudio (v1.0.153) software was used for graphing and statistical analysis of sequencing data.

1. S. M. Reppert, D. R. Weaver, Coordination of circadian timing in mammals. *Nature* **418**, 935–941 (2002).
2. J. S. Takahashi, H.-K. Hong, C. H. Ko, E. L. McDearmon, The genetics of mammalian circadian order and disorder: Implications for physiology and disease. *Nat. Rev. Genet.* **9**, 764–775 (2008).
3. J. Bass, J. S. Takahashi, Circadian integration of metabolism and energetics. *Science* **330**, 1349–1354 (2010).
4. J. Bass, M. A. Lazar, Circadian time signatures of fitness and disease. *Science* **354**, 994–999 (2016).
5. A. M. Cypess et al., Identification and importance of brown adipose tissue in adult humans. *N. Engl. J. Med.* **360**, 1509–1517 (2009).
6. W. D. van Marken Lichtenbelt et al., Cold-activated brown adipose tissue in healthy men. *N. Engl. J. Med.* **360**, 1500–1508 (2009).
7. Z. Gerhart-Hines et al., The nuclear receptor Rev-erbα controls circadian thermogenic plasticity. *Nature* **503**, 410–413 (2013).
8. F. S. M. Machado et al., Time-of-day effects on metabolic and clock-related adjustments to cold. *Front. Endocrinol.* **9**, 199 (2018).
9. S. Chappuis et al., Role of the circadian clock gene Per2 in adaptation to cold temperature. *Mol. Metab.* **2**, 184–193 (2013).
10. M. Razzoli, M. J. Emmett, M. A. Lazar, A. Bartolomucci, β-Adrenergic receptors control brown adipose UCP-1 tone and cold response without affecting its circadian rhythmicity. *FASEB J.* **32**, 5640–5646 (2018).

11. K. Tokizawa, Y. Uchida, K. Nagashima, Thermoregulation in the cold changes depending on the time of day and feeding condition: Physiological and anatomical analyses of involved circadian mechanisms. *Neuroscience* **164**, 1377–1386 (2009).

12. B. Cannon, J. Nedergaard, Brown adipose tissue: Function and physiological significance. *Physiol. Rev.* **84**, 277–359 (2004).

13. K. L. Townsend, Y.-H. Tseng, Brown fat fuel utilization and thermogenesis. *Trends Endocrinol. Metab.* **25**, 168–177 (2014).

14. M. Calderon-Dominguez et al., Fatty acid metabolism and the basis of brown adipose tissue function. *Adipocyte* **5**, 98–118 (2015).

15. D. Guan et al., Diet-induced circadian enhancer remodeling synchronizes opposing hepatic lipid metabolic processes. *Cell* **174**, 831–842.e12 (2018).

16. E. P. Mottillo et al., Coupling of lipolysis and de novo lipogenesis in brown, beige, and white adipose tissues during chronic β3-adrenergic receptor activation. *J. Lipid Res.* **55**, 2276–2286 (2014).

17. X. X. Yu, D. A. Lewin, W. Forrest, S. H. Adams, Cold elicits the simultaneous induction of fatty acid synthesis and β-oxidation in murine brown adipose tissue: Prediction from differential gene expression and confirmation in vivo. *FASEB J.* **16**, 155–168 (2002).

18. I. G. Shabalina et al., UCP1 in brite/beige adipose tissue mitochondria is functionally thermogenic. *Cell Rep.* **5**, 1196–1203 (2013).

19. K. Ikeda, P. Maretich, S. Kajimura, The common and distinct features of brown and beige adipocytes. *Trends Endocrinol. Metab.* **29**, 191–200 (2018).

20. J. D. Horton et al., Combined analysis of oligonucleotide microarray data from transgenic and knockout mice identifies direct SREBP target genes. *Proc. Natl. Acad. Sci. U.S.A.* **100**, 12027–12032 (2003).

21. J. D. Horton, J. L. Goldstein, M. S. Brown, SREBPs: Activators of the complete program of cholesterol and fatty acid synthesis in the liver. *J. Clin. Invest.* **109**, 1125–1131 (2002).

22. M. Amemiya-Kudo et al., Promoter analysis of the mouse sterol regulatory element-binding protein-1c gene. *J. Biol. Chem.* **275**, 31078–31085 (2000).

23. R. Dentin, J. Girard, C. Postic, Carbohydrate responsive element binding protein (ChREBP) and sterol regulatory element binding protein-1c (SREBP-1c): Two key regulators of glucose metabolism and lipid synthesis in liver. *Biochimie* **87**, 81–86 (2005).

24. X. Xu, J.-S. So, J.-G. Park, A.-H. Lee, Transcriptional control of hepatic lipid metabolism by SREBP and ChREBP. *Semin. Liver Dis.* **33**, 301–311 (2013).

25. M. Matsuda et al., SREBP cleavage-activating protein (SCAP) is required for increased lipid synthesis in liver induced by cholesterol deprivation and insulin elevation. *Genes Dev.* **15**, 1206–1216 (2001).

26. M. Adlanmerini, Y. Aubert, M.A. Lazar, Genome-wide mapping of HA-tagged REV-ERBα in mice Brown Adipose Tissue (BAT) after one week at thermoneutrality (29C) or exposed to chronic cold (4C). Gene Expression Omnibus. https://www.ncbi.nlm.nih.gov/geo/query/acc.cgi?acc=GSE128960. Deposited 27 March 2019.

27. P. Dierickx et al., SR9009 has REV-ERB-independent effects on cell proliferation and metabolism. *Proc. Natl. Acad. Sci. U.S.A.* **116**, 12147–12152 (2019).

28. K. Düvel et al., Activation of a metabolic gene regulatory network downstream of mTOR complex 1. *Mol. Cell* **39**, 171–183 (2010).

29. M. Laplante, D. M. Sabatini, mTORC1 activates SREBP-1c and uncouples lipogenesis from gluconeogenesis. *Proc. Natl. Acad. Sci. U.S.A.* **107**, 3281–3282 (2010).

30. M. Laplante, D. M. Sabatini, mTOR signaling in growth control and disease. *Cell* **149**, 274–293 (2012).

31. D. Liu et al., Activation of mTORC1 is essential for β-adrenergic stimulation of adipose browning. *J. Clin. Invest.* **126**, 1704–1716 (2016).

32. I. Bakan, M. Laplante, Connecting mTORC1 signaling to SREBP-1 activation. *Curr. Opin. Lipidol.* **23**, 226–234 (2012).

33. S. M. Labbé et al., mTORC1 is required for brown adipose tissue recruitment and metabolic adaptation to cold. *Sci. Rep.* **6**, 37223 (2016).

34. Y.-A. Moon et al., The Scap/SREBP pathway is essential for developing diabetic fatty liver and carbohydrate-induced hypertriglyceridemia in animals. *Cell Metab.* **15**, 240–246 (2012).

35. S. Satoh et al., Identification of cis-regulatory elements and trans-acting proteins of the rat carbohydrate response element binding protein gene. *Arch. Biochem. Biophys.* **461**, 113–122 (2007).

36. M. Rosenwald, A. Perdikari, T. Rülicke, C. Wolfrum, Bi-directional interconversion of brite and white adipocytes. *Nat. Cell Biol.* **15**, 659–667 (2013).

37. J. Terrien, P. Zizzari, J. Epelbaum, M. Perret, F. Aujard, Daily rhythms of core temperature and locomotor activity indicate different adaptive strategies to cold exposure in adult and aged mouse lemurs acclimated to a summer-like photoperiod. *Chronobiol. Int.* **26**, 838–853 (2009).

38. V. Cadena, G. J. Tattersall, Body temperature regulation during acclimation to cold and hypoxia in rats. *J. Therm. Biol.* **46**, 56–64 (2014).

39. P. M. Marvyn, R. M. Bradley, E. B. Mardian, K. A. Marks, R. E. Duncan, Data on oxygen consumption rate, respiratory exchange ratio, and movement in C57BL/6J female mice on the third day of consuming a high-fat diet. *Data Brief* **7**, 472–475 (2016).

40. H. Shin, H. Shi, B. Xue, L. Yu, What activates thermogenesis when lipid droplet lipolysis is absent in brown adipocytes? *Adipocyte* **7**, 1–5 (2018).

41. H. Shin et al., Lipolysis in brown adipocytes is not essential for cold-induced thermogenesis in mice. *Cell Metab.* **26**, 764–777.e5 (2017).

42. K. Tokizawa, T. Yoda, Y. Uchida, K. Kanosue, K. Nagashima, Estimation of the core temperature control during ambient temperature changes and the influence of circadian rhythm and metabolic conditions in mice. *J. Therm. Biol.* **51**, 47–54 (2015).

43. J. Lee, J. M. Ellis, M. J. Wolfgang, Adipose fatty acid oxidation is required for thermogenesis and potentiates oxidative stress-induced inflammation. *Cell Rep.* **10**, 266–279 (2015).

44. S. Ji et al., Homozygous carnitine palmitoyltransferase 1b (muscle isoform) deficiency is lethal in the mouse. *Mol. Genet. Metab.* **93**, 314–322 (2008).

45. M. Watanabe et al., Cold-induced changes in gene expression in brown adipose tissue: Implications for the activation of thermogenesis. *Biol. Pharm. Bull.* **31**, 775–784 (2008).

46. J. Sanchez-Gurmaches et al., Brown fat AKT2 is a cold-induced kinase that stimulates ChREBP-mediated de novo lipogenesis to optimize fuel storage and thermogenesis. *Cell Metab.* **27**, 195–209.e6 (2018).

47. S. M. Labbé et al., In vivo measurement of energy substrate contribution to cold-induced brown adipose tissue thermogenesis. *FASEB J.* **29**, 2046–2058 (2015).

48. A. Guilherme et al., Neuronal modulation of brown adipose activity through perturbation of white adipocyte lipogenesis. *Mol. Metab.* **16**, 116–125 (2018).

49. R. Schreiber et al., Cold-induced thermogenesis depends on ATGL-mediated lipolysis in cardiac muscle, but not brown adipose tissue. *Cell Metab.* **26**, 753–763.e7 (2017).

50. J. D. McGarry, G. F. Leatherman, D. W. Foster, Carnitine palmitoyltransferase I. The site of inhibition of hepatic fatty acid oxidation by malonyl-CoA. *J. Biol. Chem.* **253**, 4128–4136 (1978).

51. D. W. Foster, Malonyl-CoA: The regulator of fatty acid synthesis and oxidation. *J. Clin. Invest.* **122**, 1958–1959 (2012).

52. S. Banfi, V. Gusarova, J. Gromada, J. C. Cohen, H. H. Hobbs, Increased thermogenesis by a noncanonical pathway in ANGPTL3/8-deficient mice. *Proc. Natl. Acad. Sci. U.S.A.* **115**, E1249–E1258 (2018).

53. M. J. Emmett et al., Histone deacetylase 3 prepares brown adipose tissue for acute thermogenic challenge. *Nature* **546**, 544–548 (2017).

54. B. Cannon, J. Nedergaard, Nonshivering thermogenesis and its adequate measurement in metabolic studies. *J. Exp. Biol.* **214**, 242–253 (2011).

55. R. Papazyan et al., Physiological suppression of lipotoxic liver damage by complementary actions of HDAC3 and SCAP/SREBP. *Cell Metab.* **24**, 863–874 (2016).

56. M. E. Hughes, J. B. Hogenesch, K. Kornacker, JTK_CYCLE: An efficient nonparametric algorithm for detecting rhythmic components in genome-scale data sets. *J. Biol. Rhythms* **25**, 372–380 (2010).

PHYSIOLOGY